Discovering solid electrolytes through the analysis of machine-learned potential energy surfaces

Artem Maevskiy [1] **Alexandra Carvalho** [1 2] **Emil Sataev** [3] **Volha Turchyna** [3] **Keian Noori** [1 2]
Aleksandr Rodin [4 5] **A. H. Castro Neto** [1 2 5 6] **Andrey Ustyuzhanin** [1 7]

[1]*National University of Singapore, Institute for Functional Intelligent Materials, NUS S9 Building, 4 Science Drive 2, 117544 Singapore* [2]*National University of Singapore, Centre for Advanced 2D Materials, 6 Science Drive 2, 117546 Singapore* [3]*HSE University, Faculty of Computer Science, Pokrovsky Boulevard 11, 109028 Moscow, Russian Federation* [4]*Yale-NUS College, 16 College Avenue West, 138527 Singapore* [5]*National University of Singapore, Department of Materials Science Engineering, 9 Engineering Drive 1, 117575 Singapore* [6]*National University of Singapore, Department of Physics, 2 Science Drive 3, 117551 Singapore* [7]*Constructor University, Bremen, Campus Ring 1, 28759, Germany* . Correspondence to: Artem Maevskiy maevskiy@nus.edu.sg.

1. Introduction

Solid-state battery (SSB) technology promises improved capacity and safety compared to conventional batteries with liquid electrolytes [1–4]. This advancement has the potential to address the pressing energy storage challenges in various applications, including electric vehicles, portable electronics, and renewable energy integration [1, 4]. The widespread adoption of SSBs is, however, impeded by several obstacles. A number of challenges involve achieving and maintaining physical and chemical stability at the electrolyte-electrode interfaces [5, 6]. Moreover, there is a general limitation of ionic conductivity in solids, which tends to be lower than that of liquid electrolytes [3, 7]. Therefore, the need for new fast-conducting materials remains a major challenge in the development of SSBs [3].

Computational techniques for assessing ionic conductivities in solids pave the way for *in silico* discovery of novel superionic materials [8, 9]. Among these techniques, molecular dynamics simulations driven by forces from Kohn-Sham density functional theory (DFT), hereafter referred to as *ab initio* molecular dynamics (AIMD), allow to identify, understand, and evaluate the ion diffusion mechanisms in new materials [8]. These calculations have been successfully utilized in various studies focused on solid electrolyte discovery [10–12]. The biggest limitation of this approach is its high computational cost, which motivates the use of faster approximate screening methods on large material datasets before validating the final predictions with AIMD. For instance, such a scheme is applied in [11], where approximate diffusivity is evaluated using a simplified molecular dynamics model with lithium ions moving in a frozen host lattice (the pinball model). Similarly, Ref. [12] follows this logic, using a logistic regression model fitted to labeled data on ionic conductivity for initial screening.

In this work, we propose a heuristic approach for predicting materials with high ionic conductivity based on the analysis of the potential energy landscape observed by mobile ions. Our technique is designed to be computationally efficient and automated, making it suitable for large-scale screening of solid electrolytes. To test the method, we apply it to lithium-containing structures from the Materials Project database [13]. We find that the resulting predictions, while including well-known superionic materials like LGPS [14] or $Li_7P_3S_{11}$ [15], also contain a number of less expected candidates. In particular, our top prediction, LiB_3H_8, is a hydroborate that, to the best of our knowledge, has not been studied as a potential ionic conductor before. In fact, our method has highlighted a number of hydroborates, a known family of superionic conductors, without using any prior information regarding ionic conductivity within this family. Notably, this family is typically not present in findings from similar high-throughput searches [11, 12, 16–18], indicating that our approach complements existing methods. Figure 1 demonstrates a flowchart of logical steps performed in this study.

2. Methodology

For a given structure, we analyze the potential energy landscape observed by the mobile ion while remaining ions are fixed in their equilibrium locations. We denote this setup as the *frozen framework* approximation. We evaluate the potential energy using the M3GNet [19] model, though we expect our approach to work with other universal potential models or DFT. A discussion of the errors introduced by these approximations can be found in Appendix B. We extract various numeric features from the potential energy landscape and select those that show the highest correlation with Li conductivity in the labeled structures, as described in Appendix A. Finally, we validate our results by running AIMD simulations for the top predictions, with more details in Appendix C. For a complete description of the methodology, we direct the reader to [20].

3. Results

3.1 Accuracy based on top 10 candidates

From the top ten predicted structures, five are well-studied superionic materials derived from LGPS through element substitution [10] and are therefore excluded from our AIMD validation procedure. Of the remaining five, three — orthorhombic LiB_3H_8 (`mp-1211100`), cubic $Li(BH)_6$ (`mp-1211296`)

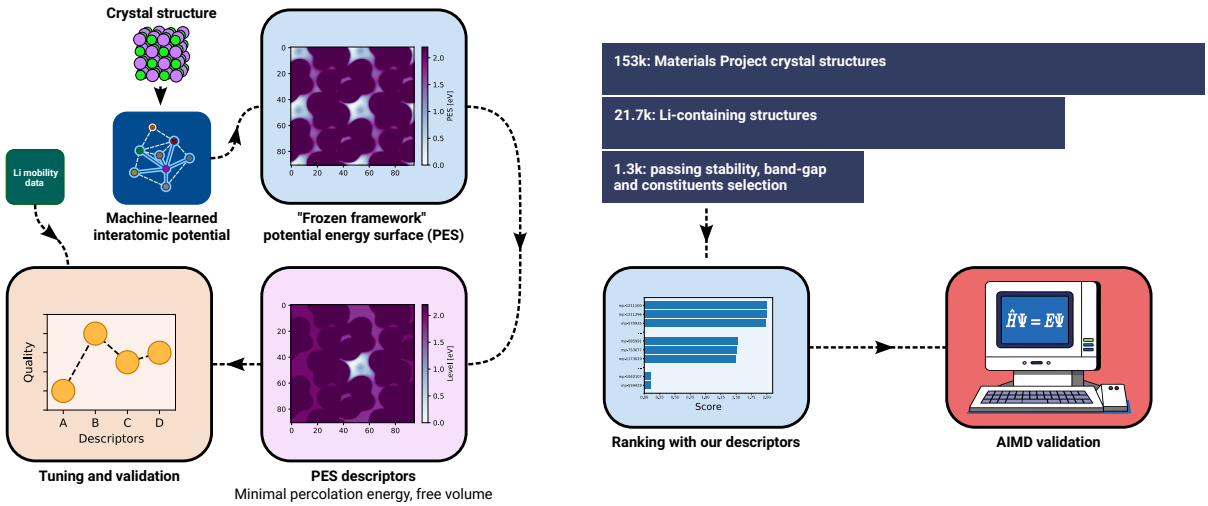

Fig. 1: Flowchart illustrating the logical steps of the study: (left) calculation and optimization of descriptors, and (right) prediction and validation of the most promising candidates

and hexagonal $LiBH_4$ (mp-644223) — demonstrate significant lithium mobility in low-temperature AIMD simulations. The other two — wurtzite LiI (mp-570935) and fluorite-structured Li_2Te (mp-2530) — are only diffusive at $T = 1000\,\mathrm{K}$, as shown in Fig. A2. Overall, this yields eight out of ten correct predictions for superionic behavior at room temperature and ten out of ten for high temperatures.

3.2 *Hydroborate candidates*

Of the lithium hydroborate predictions, the best studied is the hexagonal $LiBH_4$ [21–23]. It has been found experimentally to have an ionic conductivity of the order of $1\,\mathrm{mS/cm}$ at $T = 110\,^\circ\mathrm{C}$, below which it exists in a different phase. Cubic $Li(BH)_6$ has been found to have low diffusivity in a computational study, but a closely connected orthorhombic distortion of the structure is reported to have a conductivity of up to $0.1\,\mathrm{S/cm}$ at $700\,\mathrm{K}$ [24].

To the best of our knowledge, lithium conductivity has not been previously studied in LiB_3H_8, our top prediction. The similar NaB_3H_8 structure has recently been successfully used in a composite solid electrolyte in a sodium-metal SSB [25, 26]. Ionic conductivity and relaxation times for anionic reorientation have also been studied for various phases of the related KB_3H_8 [27, 28]. In our AIMD calculations, LiB_3H_8 has demonstrated very high conductivity at the lowest temperature simulated, $\sigma_{500\,\mathrm{K}} = 1.6 \pm 0.4\,\mathrm{S/cm}$. The fitted activation energy is $E_A = 99 \pm 93\,\mathrm{meV}$; however the R^2 for this fit is only 0.696, which doesn't allow for a reliable extrapolation to room temperature.

3.3 *Computational efficiency*

We note that our PES descriptors are very fast to calculate when compared to other methods for predicting ionic conductivity. Running our calculations on a single machine with 48-core Intel Xeon w7-3455 CPU and two 46-GB NVIDIA RTX 6000 Ada Generation GPUs yielded the average calculation speed of ~ 1.7 minutes per structure. For comparison, the same characteristic for the SevenNet [29] molecular dynamics used for additional validation described in Appendix D is of the order of ~ 100 minutes per structure. Our AIMD calculations, though run on different hardware (64 CPU cores, without GPU acceleration) and therefore not directly comparable, take between four and twelve days per structure per temperature point, depending on the material.

4. Conclusion

We have proposed an effective and computationally efficient technique for screening solid electrolyte materials through the analysis of the potential energy landscape experienced by the mobile ions. Having applied our method to lithium-containing structures from the Materials Project, we demonstrate its accuracy with ten out of ten of the highest-ranked predictions agreeing with first-principles calculations at $T = 1000\,\mathrm{K}$, and eight out of ten at room temperature. Notably, our technique has highlighted several hydroborate structures, a known family of superionic conductors, which typically evade other screening approaches. Our top prediction, LiB_3H_8, has demonstrated very high ionic mobility in AIMD calculations. To the best of our knowledge, this material has not been studied as an ionic conductor before.

The code implementing the proposed technique, as well as the predictions calculated for lithium-containing structures from the Materials Project, are available in [30].

Acknowledgments

This research project is supported by the Ministry of Education, Singapore, under its Research Centre of Excellence award to the Institute for Functional Intelligent Materials, National University of Singapore (I-FIM, project No. EDUNC-33-18-279-V12). This

work used computational resources of the Singapore National Supercomputing Centre (NSCC) of Singapore. For the exploratory phase, this work used computational resources of the Constructor Research Platform provided by Constructor Technologies.

References

[1] Joo Gon Kim, Byungrak Son, Santanu Mukherjee, Nicholas Schuppert, Alex Bates, Osung Kwon, Moon Jong Choi, Hyun Yeol Chung, and Sam Park. A review of lithium and non-lithium based solid state batteries. *J. Power Sources*, 282:299–322, 2015.

[2] Cong Li, Zhen-yu Wang, Zhen-jiang He, Yun-jiao Li, Jing Mao, Ke-hua Dai, Cheng Yan, and Junchao Zheng. An advance review of solid-state battery: challenges, progress and prospects. *SM&T*, 29:e00297, 2021.

[3] Jürgen Janek and Wolfgang G Zeier. Challenges in speeding up solid-state battery development. *Nat. Energy.*, 8(3):230–240, 2023.

[4] Nancy J Dudney, William C West, and Jagjit Nanda. *Handbook of solid state batteries*, volume 6. World Scientific, Singapore, 2nd edition, 2015.

[5] Chunguang Chen, Ming Jiang, Tao Zhou, Luc Raijmakers, Egor Vezhlev, Baolin Wu, Tobias U Schülli, Dmitri L Danilov, Yujie Wei, Rüdiger-A Eichel, et al. Interface aspects in all-solid-state Li-based batteries reviewed. *Advanced energy materials*, 11(13):2003939, 2021.

[6] Narumi Ohta, Kazunori Takada, Lianqi Zhang, Renzhi Ma, Minoru Osada, and Takayoshi Sasaki. Enhancement of the high-rate capability of solid-state lithium batteries by nanoscale interfacial modification. *Advanced Materials*, 18(17):2226–2229, 2006.

[7] Qing Zhao, Sanjuna Stalin, Chen-Zi Zhao, and Lynden A. Archer. Designing solid-state electrolytes for safe, energy-dense batteries. *Nature Reviews Materials*, 5(3):229–252, Mar 2020.

[8] Zhi Deng, Yifei Mo, and Shyue Ping Ong. Computational studies of solid-state alkali conduction in rechargeable alkali-ion batteries. *NPG Asia Materials*, 8(3):e254–e254, 2016.

[9] Zhuoying Zhu, Zhi Deng, Iek-Heng Chu, Balachandran Radhakrishnan, and Shyue Ping Ong. *Ab Initio Molecular Dynamics Studies of Fast Ion Conductors*, pages 147–168. Springer International Publishing, Cham, 2018.

[10] Shyue Ping Ong, Yifei Mo, William Davidson Richards, Lincoln Miara, Hyo Sug Lee, and Gerbrand Ceder. Phase stability, electrochemical stability and ionic conductivity of the Li10±1MP2X12 (M = Ge, Si, Sn, Al or P, and X = O, S or Se) family of superionic conductors. *Energy Environ. Sci.*, 6:148–156, 2013.

[11] Leonid Kahle, Aris Marcolongo, and Nicola Marzari. High-throughput computational screening for solid-state li-ion conductors. *Energy Environ. Sci.*, 13:928–948, 2020.

[12] Austin D Sendek, Ekin D Cubuk, Evan R Antoniuk, Gowoon Cheon, Yi Cui, and Evan J Reed. Machine learning-assisted discovery of solid Li-ion conducting materials. *Chemistry of Materials*, 31(2):342–352, 2019.

[13] Anubhav Jain, Shyue Ping Ong, Geoffroy Hautier, Wei Chen, William Davidson Richards, Stephen Dacek, Shreyas Cholia, Dan Gunter, David Skinner, Gerbrand Ceder, and Kristin A. Persson. Commentary: The materials project: A materials genome approach to accelerating materials innovation. *APL materials*, 1(1):011002, 07 2013.

[14] Noriaki Kamaya, Kenji Homma, Yuichiro Yamakawa, Masaaki Hirayama, Ryoji Kanno, Masao Yonemura, Takashi Kamiyama, Yuki Kato, Shigenori Hama, Koji Kawamoto, and Akio Mitsui. A lithium superionic conductor. *Nature materials*, 10(9):682–686, Sep 2011.

[15] Hisanori Yamane, Masatoshi Shibata, Yukio Shimane, Tadanori Junke, Yoshikatsu Seino, Stefan Adams, Keiichi Minami, Akitoshi Hayashi, and Masahiro Tatsumisago. Crystal structure of a superionic conductor, Li7P3S11. *Solid State Ionics*, 178(15):1163–1167, 2007.

[16] Yan Wang, William Davidson Richards, Shyue Ping Ong, Lincoln J Miara, Jae Chul Kim, Yifei Mo, and Gerbrand Ceder. Design principles for solid-state lithium superionic conductors. *Nature materials*, 14(10):1026–1031, Oct 2015.

[17] Sokseiha Muy, Johannes Voss, Roman Schlem, Raimund Koerver, Stefan J Sedlmaier, Filippo Maglia, Peter Lamp, Wolfgang G Zeier, and Yang Shao-Horn. High-throughput screening of solid-state Li-ion conductors using lattice-dynamics descriptors. *iScience*, 16:270–282, Jun 2019.

[18] Forrest AL Laskowski, Daniel B McHaffie, and Kimberly A See. Identification of potential solid-state li-ion conductors with semi-supervised learning. *Energy & Environmental Science*, 16(3):1264–1276, 2023.

[19] Chi Chen and Shyue Ping Ong. A universal graph deep learning interatomic potential for the periodic table. *Nature Computational Science*, 2(11):718–728, Nov 2022.

[20] Artem Maevskiy, Alexandra Carvalho, Emil Sataev, Volha Turchyna, Keian Noori, Aleksandr Rodin, A. H. Castro Neto, and Andrey Ustyuzhanin. Predicting ionic conductivity in solids from the machine-learned potential energy landscape. (arXiv:2411.06804), 2024.

[21] Motoaki Matsuo, Yuko Nakamori, Shin-ichi Orimo, Hideki Maekawa, and Hitoshi Takamura. Lithium superionic conduction in lithium borohydride accompanied by structural transition. *Applied Physics Letters*, 91(22):224103, 11 2007.

[22] Léo Duchêne, Arndt Remhof, Hans Hagemann, and Corsin Battaglia. Status and prospects of hydroborate electrolytes for all-solid-state batteries. *Energy Storage Materials*, 25:782–794, 2020.

[23] Huixiang Liu, Xian Zhou, Mingxin Ye, and Jianfeng Shen. Ion migration mechanism study of hydroborate/carborate electrolytes for all-solid-state batteries. *Electrochemical Energy Reviews*, 6(1):31, 2023.

[24] Alexey P Maltsev, Ilya V Chepkasov, and Artem R Oganov. Order–disorder phase transition and ionic conductivity in a Li2B12H12 solid electrolyte. *ACS Applied Materials & Interfaces*, 15(36):42511–42519, 2023.

[25] Pengtao Qiu, Xinwei Chen, Wanyu Zhang, Guoguo Zhang, Yichun Zhang, Zhiwei Lu, Yiying Wu, and Xuenian Chen. A High-Rate and Long-Life Sodium Metal Battery Based on a NaB3H8 · xNH3@NaB3H8 Composite Solid-State Electrolyte. *Angewandte Chemie International Edition*, 63(17):e202401480, 2024.

[26] Xin-Wei Chen, Jia-Xin Kang, Zi-Heng Fan, Na Zhang, Wan-Yu Zhang, Guo-Guo Zhang, An-Qi Zhu, Zhi-Wei Lu, Pengtao Qiu, Yiying Wu, and Xuenian Chen. Sodium octahydridotriborate as a solid electrolyte with excellent stability against sodium-metal anode. *Small*, 20(40):2401439, 2024.

[27] Jakob B. Grinderslev, Kasper T. Møller, Yigang Yan, Xi-Meng Chen, Yongtao Li, Hai-Wen Li, Wei Zhou, Jørgen Skibsted, Xuenian Chen, and Torben R. Jensen. Potassium octahydridotriborate: diverse polymorphism in a potential hydrogen storage material and potassium ion conductor. *Dalton Trans.*, 48:8872–8881, 2019.

[28] M. S. Andersson, J. B. Grinderslev, X.-M. Chen, X. Chen, U. Häussermann, W. Zhou, T. R. Jensen, M. Karlsson, and T. J. Udovic. Interplay between the Reorientational Dynamics of the B3H8- Anion and the Structure in KB3H8. *The Journal of Physical Chemistry C*, 125(7):3716–3724, 2021.

[29] Yutack Park, Jaesun Kim, Seungwoo Hwang, and Seungwu Han. Scalable parallel algorithm for graph neural network interatomic potentials in molecular dynamics simulations. *Journal of Chemical Theory and Computation*, 20(11):4857–4868, 2024. PMID: 38813770.

[30] 2024. `https://constructor.app/platform/public/project/pes_fingerprint`.

[31] Bowen Deng, Peichen Zhong, KyuJung Jun, Janosh Riebesell, Kevin Han, Christopher J. Bartel, and Gerbrand Ceder. CHGNet as a pretrained universal neural network potential for charge-informed atomistic modelling. *Nature Machine Intelligence*, 5(9):1031–1041, Sep 2023.

[32] Ilyes Batatia, Simon Batzner, Dávid Péter Kovács, Albert Musaelian, Gregor N. C. Simm, Ralf Drautz, Christoph Ortner, Boris Kozinsky, and Gábor Csányi. The design space of e(3)-equivariant atom-centered interatomic potentials. (arXiv:2205.06643), 2022.

[33] Ilyes Batatia, David Peter Kovacs, Gregor N. C. Simm, Christoph Ortner, and Gabor Csanyi. MACE: Higher order equivariant message passing neural networks for fast and accurate force fields. In Alice H. Oh, Alekh Agarwal, Danielle Belgrave, and Kyunghyun Cho, editors, *Advances in Neural Information Processing Systems*, 2022.

[34] Ilyes Batatia, Philipp Benner, Yuan Chiang, Alin M Elena, Dávid P Kovács, Janosh Riebesell, Xavier R Advincula, Mark Asta, William J Baldwin, Noam Bernstein, et al. A foundation model for atomistic materials chemistry. (arXiv:2401.00096), 2023.

[35] Janosh Riebesell, Rhys E. A. Goodall, Philipp Benner, Yuan Chiang, Bowen Deng, Alpha A. Lee, Anubhav Jain, and Kristin A. Persson. Matbench Discovery – A framework to evaluate machine learning crystal stability predictions. (arXiv:2308.14920), 2023.

[36] Koichi Momma and Fujio Izumi. *VESTA3* for three-dimensional visualization of crystal, volumetric and morphology data. *Journal of Applied Crystallography*, 44(6):1272–1276, Dec 2011.

[37] Jinzhe Zeng, Duo Zhang, Denghui Lu, Pinghui Mo, Zeyu Li, Yixiao Chen, Marián Rynik, Li'ang Huang, Ziyao Li, Shaochen Shi, Yingze Wang, Haotian Ye, Ping Tuo, Jiabin Yang, Ye Ding, Yifan Li, Davide Tisi, Qiyu Zeng, Han Bao, Yu Xia, Jiameng Huang, Koki Muraoka, Yibo Wang, Junhan Chang, Fengbo Yuan, Sigbjørn Løland Bore, Chun Cai, Yinnian Lin, Bo Wang, Jiayan Xu, Jia-Xin Zhu, Chenxing Luo, Yuzhi Zhang, Rhys E A Goodall, Wenshuo Liang, Anurag Kumar Singh, Sikai Yao, Jingchao Zhang, Renata Wentzcovitch, Jiequn Han, Jie Liu, Weile Jia, Darrin M

York, Weinan E, Roberto Car, Linfeng Zhang, and Han Wang. DeePMD-kit v2: A software package for deep potential models. *J. Chem. Phys.*, 159:054801, 2023.

[38] Ji Qi, Tsz Wai Ko, Brandon C. Wood, Tuan Anh Pham, and Shyue Ping Ong. Robust training of machine learning interatomic potentials with dimensionality reduction and stratified sampling. *npj Computational Materials*, 10(1):43, Feb 2024.

[39] Tomohide Morimoto, Masaya Nagai, Yosuke Minowa, Masaaki Ashida, Yoichiro Yokotani, Yuji Okuyama, and Yukimune Kani. Microscopic ion migration in solid electrolytes revealed by terahertz time-domain spectroscopy. *Nature communications*, 10(1):2662, 2019.

[40] Eveline van der Maas, Theodosios Famprikis, Saskia Pieters, Jonas P Dijkstra, Zhaolong Li, Steven R Parnell, Ronald I Smith, Ernst RH van Eck, Swapna Ganapathy, and Marnix Wagemaker. Re-investigating the structure–property relationship of the solid electrolytes Li_{3-x} In_{1-x} Zr_x Cl_6 and the impact of In–Zr (iv) substitution. *Journal of Materials Chemistry A*, 11(9):4559–4571, 2023.

[41] José M. Soler, Emilio Artacho, Julian D. Gale, Alberto García, Javier Junquera, Pablo Ordejón, and Daniel Sánchez-Portal. The SIESTA method for ab initio order-N materials simulation. *J. Phys.: Condens. Matter*, 14(11):2745–2779, 2002.

[42] John P. Perdew, Kieron Burke, and Matthias Ernzerhof. Generalized gradient approximation made simple. *Phys. Rev. Lett.*, 77:3865–3868, Oct 1996.

[43] Kyuho Lee, Éamonn D Murray, Lingzhu Kong, Bengt I Lundqvist, and David C Langreth. Higher-accuracy van der Waals density functional. *Physical Review B*, 82(8):081101, 2010.

[44] Max Dion, Henrik Rydberg, Elsebeth Schröder, David C Langreth, and Bengt I Lundqvist. Van der Waals Density Functional for General Geometries. *Phys. Rev. Lett.*, 92(24):246401, 2004.

[45] Norman Troullier and José Luís Martins. Efficient pseudopotentials for plane-wave calculations. *Physical Review B*, 43(3):1993, 1991.

[46] Daniel Sánchez-Portal, Pablo Ordejon, Emilio Artacho, and Jose M Soler. Density-functional method for very large systems with lcao basis sets. *International journal of quantum chemistry*, 65(5):453–461, 1997.

[47] Daniel Sánchez-Portal, Javier Junquera, Óscar Paz, and Emilio Artacho. Numerical atomic orbitals for linear-scaling calculations. *Phys. Rev. B*, 64(23):235111, 2001.

[48] Shuichi Nosé. A unified formulation of the constant temperature molecular dynamics methods. *J. Chem. Phys.*, 81(1):511–519, 1984.

[49] Martin R Busche, Dominik A Weber, Yannik Schneider, Christian Dietrich, Sebastian Wenzel, Thomas Leichtweiss, Daniel Schröder, Wenbo Zhang, Harald Weigand, Dirk Walter, Stefan J Sedlmaier, Diane Houtarde, Linda F Nazar, and Jürgen Janek. In situ monitoring of fast Li-ion conductor Li7P3S11 crystallization inside a hot-press setup. *Chemistry of Materials*, 28(17):6152–6165, 2016.

[50] Fuminori Mizuno, Akitoshi Hayashi, Kiyoharu Tadanaga, and Masahiro Tatsumisago. High lithium ion conducting glass-ceramics in the system Li2S–P2S5. *Solid State Ionics*, 177(26-32):2721–2725, 2006.

Appendix A. Potential energy surface analysis

In recent years, several machine learning models have been developed to successfully approximate the *ab initio* interatomic potential given the atomic structure [19, 29, 31–34]. Trained on extensive datasets of DFT structural relaxations [13] and covering most elements in the periodic table relevant to applications, these models are often referred to as *universal potentials* [35]. Throughout this work, we use one of such models, M3GNet [19], to calculate potential energy surface (PES) values for the studied structures.

Inspired by the frozen host lattice idea behind the pinball model from [11], our method evaluates the PES as a function of a single mobile ion's position, with the remaining ions fixed in their locations from the original relaxed structure. We refer to this approximation as the *frozen framework* approximation. In contrast to the pinball model, however, we assess this static picture without time integration. We evaluate the PES on a discrete grid of possible locations spanning the entire unit cell and calculate characteristics of the resulting landscape.

These characteristics are designed to correlate with ionic conductivity. In particular, we find the minimum-energy migration path and calculate the associated barrier, referred to as the *minimal percolation energy* (MPE). Additionally, we calculate the fractional volume of the set of locations $\vec{r}$ with energy below a given threshold τ, denoted as the *free volume* (FV), which is defined in two variations. The first variation, referred to as *disconnected*, considers any (potentially disconnected) set of such locations:

$$\mathrm{FV}_{\tau}^{\mathrm{disc.}} = \frac{|\{\vec{r} : \mathrm{PES}(\vec{r}) < \tau\}|}{|\{\vec{r}\}|}. \tag{A1}$$

The second variation, denoted as *connected*, $\mathrm{FV}_{\tau}^{\mathrm{con.}}$, includes only the connected subset of $\{\vec{r} : \mathrm{PES}(\vec{r}) < \tau\}$ that contains the ion's original

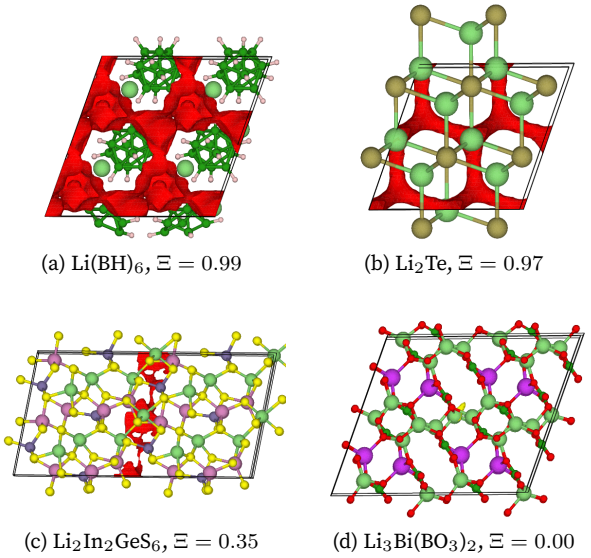

(a) $Li(BH)_6$, $\Xi = 0.99$ (b) Li_2Te, $\Xi = 0.97$

(c) $Li_2In_2GeS_6$, $\Xi = 0.35$ (d) $Li_3Bi(BO_3)_2$, $\Xi = 0.00$

Fig. A1: Volumes defining one of the most powerful *free volume* descriptors, $\mathrm{FV}^{\mathrm{con.}}_{\tau=0.5\,\mathrm{eV}}$, for various structures. Each subplot shows the connected subset of $\{\vec{r} : \mathrm{PES}(\vec{r}) < 0.5\,\mathrm{eV}\}$ containing the mobile ion's original site, where $\vec{r}$ denotes the mobile ion location at which the potential energy surface (PES) is evaluated. The isosurfaces are shown in red everywhere except (d), where yellow color is used for the isosurface and red is reserved to denote the oxygen atoms. Visualized using [36].

minimum-energy location. Figure A1 shows such connected subsets for various structures.

We use the available ionic conductivity data, both experimental [18] and computational [11], to validate the MPE and FV descriptors, as well as to optimize the energy threshold τ used in the definition of FV. From this analysis, we conclude that all proposed PES descriptors (with τ for FV ranging from 0.1 eV to 4 eV) demonstrate predictive power in identifying superionic materials. Notably, both $\mathrm{FV}^{\mathrm{con.}}_{\tau=0.5\,\mathrm{eV}}$ and $\mathrm{FV}^{\mathrm{disc.}}_{\tau=0.5\,\mathrm{eV}}$ outperform all other descriptors, although there is no clear winner between the two.

We define a positive prediction by requiring that both $\mathrm{FV}^{\mathrm{con.}}_{\tau=0.5\,\mathrm{eV}}$ and $\mathrm{FV}^{\mathrm{disc.}}_{\tau=0.5\,\mathrm{eV}}$ exceed certain cutoff values tuned on the labeled data. To allow for material ranking, we smooth these cutoffs using sigmoid functions and calculate their product, resulting in the combined ranking descriptor Ξ:

$$\begin{aligned} \Xi &= S_1 \cdot S_2, \\ S_1 &= s_{10}\left[2.00 + \log_{10} \mathrm{FV}^{\mathrm{con.}}_{\tau=0.5\,\mathrm{eV}}\right], \\ S_2 &= s_{10}\left[1.15 + \log_{10} \mathrm{FV}^{\mathrm{disc.}}_{\tau=0.5\,\mathrm{eV}}\right], \\ s_{10}(x) &\equiv \frac{1}{1+e^{-10x}}. \end{aligned} \tag{A2}$$

This descriptor is used to predict lithium superionic materials within the Materials Project database. We calculate our predictors for all lithium-containing structures with band gap above 0.5 eV and energy above hull of at most 0.05 eV / atom, excluding structures containing transition metals to enhance stability against reduction, as done in [12]. This results in 1302 structures, with 113 of them having both FV values above the cutoff values.

Appendix B. On the errors introduced by the used approximations

The use of machine-learned interatomic potentials for PES evaluation introduces errors associated with the prediction accuracy of the underlying machine learning model. For the M3GNet potential used in this work, the mean absolute error in energy prediction on the Materials Project data, relative to *ab initio* relaxation energies, is reported as 34.7 ± 3.1 meV / atom [19]. Applying the model outside its training domain can notably deteriorate accuracy, a phenomenon typically referred to as *generalization error*. For instance, in molecular dynamics simulations driven by learned potentials, this issue is typically addressed through active learning [37, 38]. In our approach, however, the structures are intentionally kept close to the training domain due to the frozen framework approximation: during PES evaluation, only a single ion location is changed compared to the relaxed Materials Project structure. We expect that this will minimize the generalization error.

The frozen framework approximation is expected to steepen the potential landscape compared to that of a realistic system. Experimental studies of superionic conductors have demonstrated that ionic hopping in these materials occurs on a timescale of ns [39, 40], allowing for the relaxation of the remaining ions and softening of the potential landscape. However, we hypothesize that frozen framework PES reflects the strength of interactions experienced during ionic hopping. This hypothesis is supported by the observed predictive power of the MPE and FV descriptors, as discussed above, based on the conductivity labels in both experimental and simulated data.

Appendix C. *Ab initio* molecular dynamics validation

AIMD simulation is carried out for the structures with the highest Ξ values. From the top ten predictions, we exclude five well-studied superionic materials derived from LGPS through element substitution [10] and perform validation only for the remaining five materials. Additionally, we simulate one reference material, a known superionic conductor, $Li_7P_3S_{11}$, which is ranked twelfth by the Ξ descriptor.

The calculations are conducted using the SIESTA code [41]. The forces are calculated using the generalized gradient approximation (GGA) of density

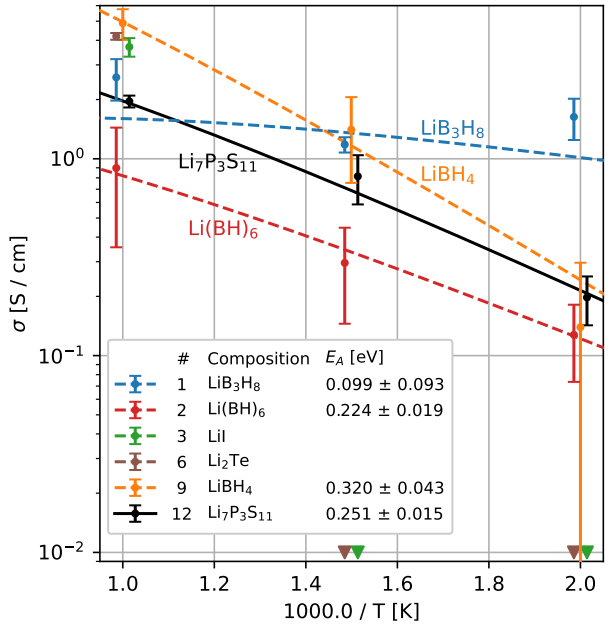

Fig. A2: Conductivity as a function of $1/T$ for the top-Ξ structures. Values below 10^{-2} S / cm are indicated with triangles. Small horizontal shifts are added to the points to enhance marker visibility. The five well-studied LGPS-like superionic materials from the top-Ξ list are omitted from our AIMD studies and therefore not shown.

functional theory [42], except for molecular solids, for which we used the LMKLL parameterization [43] of the van der Waals functional of Dion et al. [44]. The core electrons are represented by pseudopotentials of the Troullier-Martins scheme [45]. The basis sets for the Kohn-Sham states are linear combinations of numerical atomic orbitals of the polarized double-zeta type [46, 47].

We perform molecular dynamics simulations in the NVT ensemble using a Nosé thermostat [48] at three constant temperature values: 1000 K, 667 K, and 500 K. The diffusion coefficient is extracted from the ion mean squared displacement, assuming three-dimensional Brownian motion. We then connect the diffusion coefficient to the conductivity using the Nernst-Einstein relation. The obtained conductivity values are shown in Fig. A2 as a function of $1/T$.

The results of our validation procedure are consistent with the range of experimental measurements for the reference $Li_7P_3S_{11}$ structure. The extracted activation barrier and extrapolated room-temperature conductivity are $E_A = 251 \pm 15$ meV and $\sigma_{RT} = 7.4 \pm 2.9$ mS / cm. In experimental measurements, these are $E_A = 295$ meV and $\sigma_{RT} = 8.3$ mS / cm for the most pure phase sample in Ref. [49], and $E_A = 124$ meV and $\sigma_{RT} = 3.2$ mS / cm for the lowest activation barrier measurement from [50].

Appendix D. Larger-scale validation using machine-learned potential

To validate our predictions at a larger scale, we perform faster but less reliable molecular dynamics calculations driven by one of the recent universal potential models, SevenNet [29], on the 100 largest-Ξ predictions. Details for this procedure are provided in [20]. Overall, SevenNet molecular dynamics confirms 55% of our predictions to be superionic at room temperature and 88% at $T = 1000$ K. Table A1 lists our predicted materials that are confirmed to be room-temperature superionic with SevenNet molecular dynamics and that have not been predicted in Refs. [12, 17, 18].

MP identifier	Composition	Ξ
mp-1211100	LiB_3H_8	0.992
mp-1211296	$Li(BH)_6$	0.99
mp-985583	Li_3PS_4	0.958
mp-1001069	$Li_{48}P_{16}S_{61}$	0.956
mp-1097034	$Li_{20}Si_3P_3S_{23}Cl$	0.951
mp-1040451	$Li_{20}Si_3P_3S_{23}Cl$	0.949
mp-1097036	Li_3PS_4	0.931
mp-1222398	$LiGa(GeSe_3)_2$	0.896
mp-755463	Li_3SbS_3	0.887
mp-753720	Li_3BiS_3	0.858
mp-34038	Li_6NCl_3	0.814
mp-680395	Li_3As_7	0.783
mp-775806	Li_3SbS_3	0.763
mp-28336	Li_3P_7	0.721
mp-1222582	Li_4GeS_4	0.717
mp-753429	$Li_4Bi_2S_7$	0.716
mp-985582	Li_6PS_5I	0.703
mp-1177520	Li_3SbS_3	0.658
mp-1211362	$Li(BH)_6$	0.647
mp-1211446	Li_7PSe_6	0.606
mp-1222482	Li_6AsS_5I	0.539
mp-1211324	Li_7PS_6	0.538
mp-1195718	Li_4SnS_4	0.525
mp-950995	Li_6PS_5I	0.521
mp-1211176	Li_6AsS_5I	0.483

Table A1: Structures from the top-100 highest Ξ list confirmed with molecular dynamics calculations driven by the SevenNet universal potential, excluding those predicted in Refs. [12, 17, 18].